Three-Dimensional Structure in Solution of the Calcium Channel Blocker ω-Conotoxin MVIIA[†,‡]

Toshiyuki Kohno,[*,§] Jae Il Kim,[§] Kuniko Kobayashi,[§] Yoshio Kodera,[§,||] Tadakazu Maeda,[§,||] and Kazuki Sato[§]

Mitsubishi Kasei Institute of Life Sciences, Minamiooya, Machida-shi, Tokyo 194, Japan, and Department of Physics, Kitasato University, Kitasato, Sagamihara-shi, Kanagawa 228, Japan

Received April 4, 1995; Revised Manuscript Received June 1, 1995[⊗]

ABSTRACT: The three-dimensional solution structure of ω-conotoxin MVIIA, a 25-mer peptide antagonist of N-type calcium channels, was determined by two-dimensional ^{1}H NMR spectroscopy with simulated annealing calculations. A total of 13 converged structures of ω-conotoxin MVIIA were obtained on the basis of 273 experimental constraints, including 232 distance constraints obtained from nuclear Overhauser effect (NOE) connectivities, 22 torsion angle (ϕ, χ^1) constraints, and 19 constraints associated with hydrogen bonds and disulfide bonds. The atomic root mean square difference about the averaged coordinate positions is 0.47 ± 0.08 Å for the backbone atoms (N, C^α, C) and 1.27 ± 0.14 Å for all heavy atoms of the entire peptide. The molecular structure of ω-conotoxin MVIIA is composed of a short triple-stranded antiparallel β-sheet. The overall β-sheet topology is +2x, −1, which is the same as that reported for ω-conotoxin GVIA, another N-type calcium channel blocker. The orientation of β-stranded structure is similar to each other, suggesting that the conserved disulfide bond combination is essential for the molecular folding. We have recently determined by using alanine substitution analyses that Tyr 13 is essential for the activity of both toxins. On the basis of functional and structural analysis, it is shown that both ω-conotoxin MVIIA and GVIA retain a similar conformation to locate Tyr 13 in the appropriate position to allow binding to N-type calcium channels. These results provide a molecular basis for understanding the mechanism of calcium channel modulation through the toxin−channel interaction and insight into the discrimination of different subtypes of calcium channels.

Fish-hunting cone snails (*Conus*) elaborate a series of polypeptide toxins to paralyze their prey very rapidly. Many of these toxins specifically block ion channels and neurotransmitter receptors and have been used for analysis of the function of their pharmacological targets (Adams & Olivera, 1994). Among these peptide toxins, ω-conotoxin MVIIA (ω-CTX MVIIA)[1] obtained from *Conus magus* (Olivera et al., 1987) and ω-CTX GVIA (ω-conotoxin GVIA) from *Conus geographus* (Olivera et al., 1984) are specific antagonists for N-type calcium channels. ω-CTX MVIIA and ω-CTX GVIA consist of 25 and 27 amino acid residues with three disulfide bonds, respectively, but these two peptides have only about 20% homology except for cysteine residues which form disulfide bonds (Figure 1).

Recently, the three-dimensional structure of ω-CTX GVIA was determined by using NMR spectroscopy (Davis et al., 1993; Pallaghy et al., 1993; Sevilla et al., 1993; Skalicky et al., 1993); however, that of ω-CTX MVIIA has not been reported yet. Although ω-CTX MVIIA is less widely used than ω-CTX GVIA, which is a standard pharmacological tool to identify the N-type calcium channel, elucidation of its three-dimensional structure is very important for study of the specificity of its interaction with calcium channels for the following reasons.

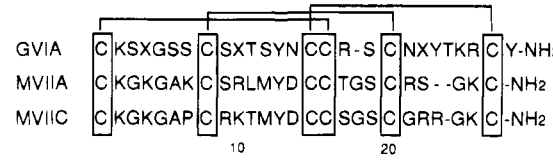

FIGURE 1: Amino acid sequences and disulfide bonds of ω-conotoxin GVIA, MVIIA, and MVIIC (X = Hyp).

Calcium channels have been classified into several subtypes according to their specific ligands such as dihydropyridine derivatives for the L-type channel, ω-CTX GVIA and MVIIA for the N-type channel, ω-agatoxin IVA for the P-type channel, and ω-CTX MVIIC for the Q-type channel (Birnbaumer et al., 1994; Olivera et al., 1994). The amino acid sequence of ω-CTX MVIIA is much more similar to that of ω-CTX MVIIC than to that of ω-CTX GVIA, although its pharmacological specificity is different from that of ω-CTX MVIIC (Figure 1). Therefore, in order to study in detail the structural differences that determine toxin selectivity for N- and Q-type calcium channels, ω-CTX MVIIA is the most appropriate representative of the N-type calcium channel blockers.

To identify the functional residues of ω-CTXs, we have synthesized numerous analogs and reported that Tyr 13 is

[†] This work was supported in part by a project grant from the Japan Health Science Foundation.

[‡] Atomic coordinates for the 13 converged structures of ω-CTX MVIIA have been deposited with Protein Data Bank, Brookhaven National Laboratories, Long Island, NY 11973, under the accession code 1OMG.

* To whom correspondence should be addressed. Fax: +81(427)-24-6317.

[§] Mitsubishi Kasei Institute of Life Sciences.

[||] Kitasato University.

[⊗] Abstract published in *Advance ACS Abstracts,* July 15, 1995.

[1] Abbreviations: ω-CTX, ω-conotoxin; NMR, nuclear magnetic resonance; COSY, correlation spectroscopy; PE-COSY, primitive exclusive COSY; DQF-COSY, double quantum-filtered COSY; TOCSY, total correlated spectroscopy; NOESY, nuclear Overhauser effect spectroscopy; RMSD, root-mean-squared deviation; Hyp, hydroxyproline. Standard abbreviations are used for usual amino acids.

0006-2960/95/0434-10256$09.00/0

essential for the activity of both ω-CTX GVIA and MVIIA (Kim et al., 1994, 1995). Lys 2 is also important for the activity of ω-CTX GVIA (Sato et al., 1993), but its role is less critical in ω-CTX MVIIA (Kim et al., 1995). These results suggest that the topology of ω-CTX MVIIA binding to the N-type calcium channel may slightly differ from that of ω-CTX GVIA. Three-dimensional structural analysis of ω-CTX MVIIA should also answer this question.

In the present study, the three-dimensional structure of ω-CTX MVIIA in aqueous solution was determined by using two-dimensional ^{1}H-NMR with simulated annealing calculations. On the basis of the analysis of the determined secondary and tertiary structure elements, the solution conformation of ω-CTX MVIIA is similar to that of ω-CTX GVIA reported previously (Davis et al., 1993; Pallaghy et al., 1993; Sevilla et al., 1993; Skalicky et al., 1993) except for the length of β-sheet and some turns. The comparison of structures of the two conotoxins and the structure–function relationships of calcium channel blockers will also be discussed.

MATERIALS AND METHODS

Materials. ω-CTX MVIIA was chemically synthesized in a large quantity by the same strategy as described previously (Kim et al., 1995). Primary structure and the purity of the synthetic peptide was confirmed by analytical HPLC, amino acid analysis, and FAB-MAS measurement.

NMR Spectroscopy. The samples for NMR experiments were prepared at a concentration of approximately 7 mM in either 99.96% ^2H_2O or 90% H_2O/10% ^2H_2O at pH 3.5. NMR measurements were performed using standard pulse sequences and phase cycling on a Bruker AMX-500 spectrometer operating at 500 MHz for the proton frequency. All two-dimensional NMR spectra were acquired in a phase-sensitive mode using time-proportional phase incrementation (Marion & Wüthrich, 1983) for quadrature detection in the t_1 dimension. NOESY spectra (Jeener et al., 1979; Macura et al., 1981) were recorded at temperatures of 15 and 25 °C with mixing times of 100, 200, and 300 ms, respectively. TOCSY spectra were recorded using a MLEV-17 pulse scheme (Bax & Davis, 1985) with isotropic mixing times of 50 and 80 ms. DQF-COSY (Rance et al., 1983) and PE-COSY (Mueller, 1987) spectra were recorded to obtain the constraints for torsion angle and stereospecific assignment. Selective irradiation during the relaxation delay period was used to suppress the solvent resonance. Data size used for all measurements was 512 (t_1) × 2048 (t_2) (512 × 8192 for PE-COSY) and spectral width was 6000 Hz.

Data processing was performed either on a Bruker X-32 UNIX workstation with UXNMR software or on a Kubota Titan 750V with NMRZ software (New Methods Research Inc.). Phase-shifted sine-squared window functions were applied prior to Fourier transformation, with shifts of π/3 to π/2 in both dimensions. Final matrix sizes were usually 2048 × 2048 real points (1024 × 8192 for PE-COSY).

For slowly exchanging backbone amide protons, the sample lyophilized from H_2O was redissolved in ^2H_2O and identified by analysis of TOCSY spectra recorded at time scales of 0.5, 3.0, 6.0, and 12 h. Chemical shifts were referenced to the methyl resonance of 3-(trimethylsilyl)-propionate-*2,2,3,3-$^2H_4$* (TSP) used as an internal standard. A complete set of the two-dimensional spectra was recorded at 15 °C and pH 3.5 (uncorrected meter readings).

Distance Constraints and Structure Calculations. Interproton distance restraints were obtained from the NOESY spectra with mixing times of either 100 or 300 ms. Quantitative determination of cross-peak intensities was based on the counting of the exponentially spaced contour levels. All NOE data were divided into three classes, strong, medium, and weak, corresponding to distance upper limits of 2.5, 3.5, and 5.0 Å in the interproton distance restraints. Pseudoatoms were used for nonstereospecifically assigned protons, and intraresidue and long-range correcting factors were added to the distance restraints, respectively (Wüthrich et al., 1983). In addition, 0.5 Å was added to the upper limits for distance restraints involving methyl protons (Clore et al., 1987). Nine additional constraints were added to define the three disulfide bonds involved in ω-CTX MVIIA. For each disulfide bond, there are three distance constraints, S(i)–S(j), S(i)–C$^\beta$(j), and S(j)–C$^\beta$(i), whose target values were set to 2.02 ± 0.02, 2.99 ± 0.5, and 2.99 ± 0.5 Å, respectively (Nilges et al., 1988). After the initial calculation, 10 distance constraints for hydrogen bonds in the β-sheet which were unambiguously defined were added as target values of 1.8–2.3 Å for NH(i)–O(j) and 2.8–3.3 Å for N(i)–O(j), respectively.

All calculations were carried out on a HP 9000/720 workstation with the X-PLOR 3.1 program (Brünger, 1993). The three-dimensional structures were calculated on the basis of the experimentally derived distance and torsion angle constraints using a dynamical simulated annealing protocol starting from a template structure with randomized backbone φ and ψ torsion angles. For structural comparison, the coordinates of ω-CTX GVIA were obtained from the Brookhaven Protein Data Bank Entry 1OMC (Davis et al., 1993).

Evaluation Methods. The convergence of the calculated structures was evaluated in terms of the structural parameters, i.e., RMS deviations from experimental distance and dihedral constraints, the values of energetic statistics (F_{NOE}, F_{tor}, F_{repel}, and $E_{L\text{-}J}$), and RMS deviations from idealized geometry. The distribution of backbone dihedral angles of the final converged structures were evaluated by the representation of the Ramachandran dihedral pattern, indicating the deviations from the sterically allowed (φ,ψ) angle limits (Ramachandran et al., 1963). The degree of angular variation among the converged structures were further assessed by using an angular order parameter S (Davis et al., 1993; Hyberts et al., 1992). The order parameter S was calculated by using

$$S = \frac{1}{N}[(\sum_{j=1}^{N}\sin\theta_j)^2 + (\sum_{j=1}^{N}\cos\theta_j)^2]^{1/2}$$

N is the number of total converged structures. θ_j is a particular dihedral angle of the jth structure of the total structures. The order parameter S for each residue shows whether the region around the residue is well defined from the point of the φ and ψ dihedral angles.

RESULTS

Sequential Resonance Assignments. Sequence-specific resonance assignments were achieved according to the standard method established by Wüthrich and co-workers (1986). The proton resonances of ω-CTX MVIIA were assigned to the spin systems of specific amino acid types by

analyzing scalar coupling patterns observed in DQF-COSY and TOCSY spectra. The identified spin systems were then aligned along the primary structure of the molecule through interresidue sequential NOEs observed on the NOESY spectra. Interresidue sequential connectivities were carried out by analysis of the $C^{\alpha}H(i)-NH(i+1)$ ($d_{\alpha N}$), $NH(i)-NH(i+1)$ (d_{NN}), and $C^{\beta}H(i)-NH(i+1)$ ($d_{\beta N}$) NOEs.

Since Ala, Leu, Met, Tyr, Asp, and Thr are present only once in the primary sequence of ω-CTX MVIIA, these residues were used as starting points for the sequential assignment process. In particular, the assignment of Ala 6, Tyr 13, and Thr 17 resonances were straightforward. The spin system for Ala 6 and Thr 17 residues were assigned through the observation of strong cross-peaks between methyl protons and $C^{\alpha}H/C^{\beta}H$, respectively, in the DQF-COSY spectrum and the magnetization transfer from $C^{\alpha}H$ to $C^{\beta}H_3$ for Ala and that from $C^{\alpha}H$ through $C^{\beta}H$ to $C^{\gamma}H_3$ for Thr in the TOCSY spectrum. The Tyr 13 residue is the only aromatic amino acid present in the primary sequence of ω-CTX MVIIA. The ring $C^{\delta}H$ resonance was assigned in the aromatic region of the DQF-COSY and TOCSY spectra and connected to the $C^{\beta}H_2$ and $C^{\alpha}H$ resonances by the NOE cross-peaks in the NOESY spectrum.

Figure 2A shows the $C^{\alpha}H-NH$ fingerprint region of the NOESY spectrum containing sequential $d_{\alpha N}(i,i+1)$ connectivities. It was possible to distinguish interresidue from intraresidue NOE cross-peaks in the NOESY spectrum by comparing the same region of the TOCSY and DQF-COSY spectra (Figure 2B). The complete sequence-specific resonance assignments of ω-CTX MVIIA are summarized in Supporting Information. Figure 3 represents sequential NOE connectivities observed in the 300 ms NOESY spectrum together with slowly exchanging amide protons and chemical shift index.

Dihedral Angles and Stereospecific Assignments. The backbone $NH-C^{\alpha}H$ coupling constants were estimated on the DQF-COSY spectrum and were converted to backbone torsion angle ϕ constraints according to the following rules: for $^3J_{NH-C^{\alpha}H}$ less than 5.5 Hz constrained the ϕ angle in the range of $-65 \pm 25°$, and for $^3J_{NH-C^{\alpha}H}$ greater than 8.0 Hz constrained in the range of $-120 \pm 40°$ (Pardi et al., 1984). Five residues (Lys 4, Ala 6, Arg 10, Cys 16, and Cys 25) with $^3J_{NH-C^{\alpha}H}$ less than 5.5 Hz and 10 residues (Lys 2, Cys 8, Ser 9, Met 12, Asp 14, Cys 15, Thr 17, Ser 19, Arg 21, and Lys 24) with $^3J_{NH-C^{\alpha}H}$ greater than 8.0 Hz, a total of 15 backbone torsion ϕ angles for ω-CTX MVIIA were constrained. Backbone dihedral constraints were not applied for $^3J_{NH-C^{\alpha}H}$ values between 5.5 and 8.0 Hz.

The range of χ^1 side chain torsion angle constraints and stereospecfic assignment of prochiral β-methylene protons were obtained by using $^3J_{\alpha\beta}$ coupling constants combined with the intraresidue $NH-C^{\beta}H$ NOEs observed with a mixing time of 100 ms (Hyberts et al., 1987). The $^3J_{\alpha\beta}$ coupling constants were determined by observing the PE-COSY spectrum in ^2H_2O, in which the cross-peaks gave the passive coupling between C^{α} and C^{β} protons. Using this procedure, we have established the stereospecific assignments together with the conformation around $C^{\alpha}-C^{\beta}$ bonds for 7 of the 14 nondegenerate β-methylene protons in ω-CTX MVIIA, i.e., Cys 1, Cys 8, Cys 15, Cys 16, Cys 20, Lys 24, and Cys 25 residues. For t^2g^3, g^2g^3, and g^2t^3 conformations around $C^{\alpha}-C^{\beta}$ bonds, the χ^1 side chain torsion angle was constrained in the range of $-60 \pm 40°$, $60 \pm 40°$, and $180 \pm 40°$, respectively (Wagner et al., 1987).

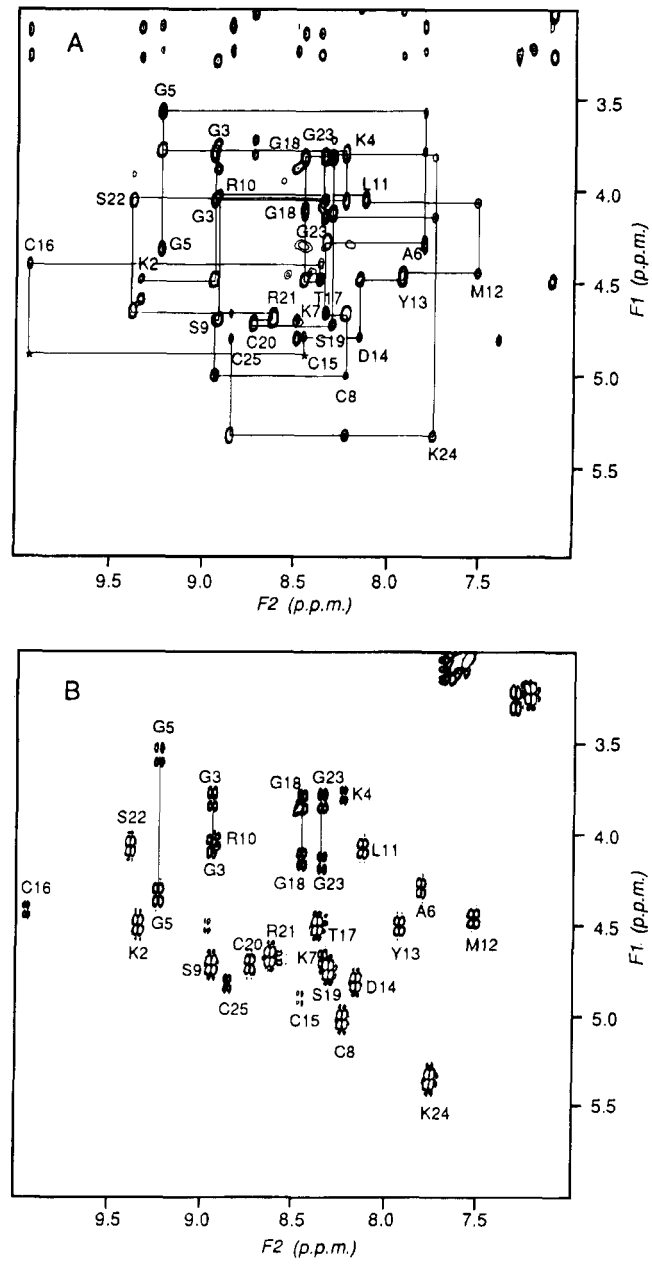

FIGURE 2: Portions of the 500 MHz two-dimensional NMR spectra of 7.0 mM ω-CTX MVIIA in 90% H_2O/10% ^2H_2O at pH 3.5 and 15 °C. (A) Sequential $d_{\alpha N}(i,i+1)$ NOE connectivities for residues from 1 to 25 in the NOESY spectrum observed with a mixing time of 300 ms. (B) Fingerprint region of the DQF-COSY spectrum corresponding to the same region as in spectrum A. In two spectral portions, the intraresidue $NH-C^{\alpha}H$ cross-peaks are labeled with the residue number by standard single-letter amino acid abbreviations.

These dihedral angles and stereospecifically assigned constraints improve the quality of the procedure for calculation of the local backbone structure and side chain conformation (Hyberts et al., 1987).

Secondary Structure. The regular secondary structure elements of the ω-CTX MVIIA molecule were identified according to standard criteria (Wüthrich et al., 1984). The extent and relative orientation of β-strands was based on large $^3J_{NH-C^{\alpha}H}$ coupling constants, strong sequential $d_{\alpha N}$, interstrand $NH-NH$ and $NH-C^{\alpha}H$ connectivities, and slowly exchang-

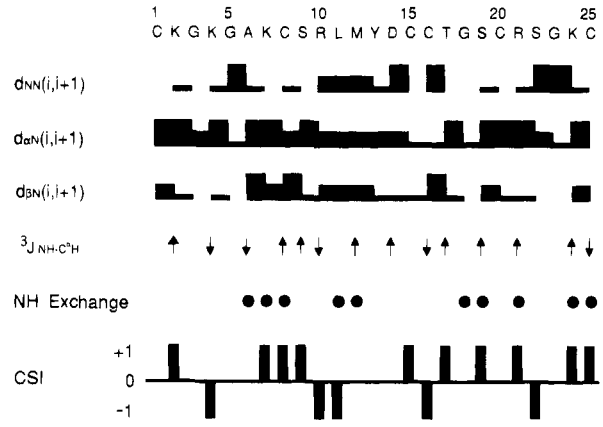

FIGURE 3: Summary of the sequential NOE connectivities, $^3J_{NH-C^\alpha H}$ coupling constants, and slowly exchanging backbone NH protons observed in ω-CTX MVIIA. These structural parameters were used for the sequence-specific assignments and the identification of secondary structure elements in ω-CTX MVIIA. The sequential NOEs, d_{NN}, $d_{\alpha N}$, and $d_{\beta N}$ are indicated by bars between two residues. The NOEs are classified into strong, medium, and weak according to the height of the filled bars. Values of $^3J_{NH-C^\alpha H}$ coupling constants are indicated by ↑ (>8.0 Hz) and ↓ (<5.5 Hz) symbols. Slowly exchanging backbone amide protons that are still observed in a TOCSY spectrum recorded after 12 h in ^2H_2O solution are indicated by filled circles. The chemical shift index is indicated by a ternary index with values of −1, 0, and +1. The values of −1 and +1 indicated a shift deviation from the random-coil value of greater than 0.1 ppm upfield and downfield, respectively, whereas those within the range of random-coil value are indicated by 0 (Wishart et al., 1992).

ing amide protons that give a discrimination of the peripheral and central strands in the β-sheet. The representation of the $C^\alpha H$ chemical shift also served as a good indicator, identifying the presence or location of secondary protein structure by using the comparative deviation of the chemical shifts of $C^\alpha H$ from those in random-coil structure (Wishart et al., 1992). On the basis of the results summarized in Figure 3, we identified three short three β-strands with residues Ala 6 to Cys 8, Ser 19 to Arg 21, and Lys 24 to Cys 25, which are arranged in an antiparallel fashion, and several turns that will be described in detail later. The analysis of the $C^\alpha H$ chemical shifts was compatible with the three-stranded antiparallel β-sheet, in which most of residues showed downfield shifts. Figure 4 shows the β-sheet region in a good agreement with the standard criteria mentioned above.

Structure Calculations and Evaluation. To determine the three-dimensional structure of ω-CTX MVIIA in solution, we carried out the structural calculation using X-PLOR simulated annealing protocol. The input data of the NMR experimental constraints consisted of 251 distance and 22 dihedral constraints. All 251 distance constraints include 89 intraresidue and 143 interresidue NOE distance constraints and an additional 19 constraints derived from hydrogen and disulfide bonds.

Simulated annealing calculations were started from 100 initial random structures and resulted in 13 final solution structures. The conformational space of the 13 final converged structures allowed by combinations of empirical energy functions and experimental data showed good agreement with the NMR input constraints, in which the NOE distance and torsion angle violations were smaller than 0.5 Å and 5°, respectively. Structural statistics for the mean and 13 converged structures were evaluated in terms of structural parameters, as shown in Table 1. The deviations from

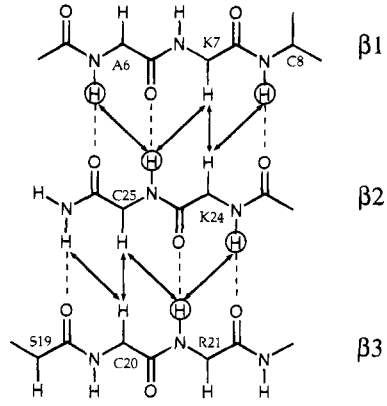

FIGURE 4: Schematic representation of the triple-stranded antiparallel β-sheet as determined by analysis of NOE connectivities, $^3J_{NH-C^\alpha H}$ coupling constants, and backbone amide proton exchange data. Observed interstrand NOEs are represented by arrows and hydrogen bonds by broken lines. Slowly exchanging backbone amide protons which are still present in a TOCSY spectrum recorded after 12 h in ^2H_2O solution are circled.

idealized covalent geometry were very small, and the Lennard-Jones van der Waals energy was large and negative, indicating that no distortions and no nonbonded bad contacts existed in the converged structures. The convergence was further assessed by the (ϕ,ψ) spacing for all selected structures. In a Ramachandran-type plot (Figure 5), the backbone dihedral angles for the all residues of the final 13 converged structures fall either in the β-sheet region or in generally allowed regions.

The overall convergence for the final set of 13 structures can be exhibited by an atomic RMSD value. The RMS differences from the averaged coordinate positions was 0.47 ± 0.08 Å for the backbone atoms (N, C^α, C) and 1.27 ± 0.14 Å for all heavy atoms. For the same atom selection, the average pairwise RMSD of the 13 individual structures was 0.68 ± 0.18 and 1.85 ± 0.28 Å, respectively (Table 2). Figure 6 panels B and C show the distribution of the atomic RMSD for the 13 converged structures about the mean structure as a function of the residue number. The backbone structure is well defined through entire residues of the molecule. However, the atomic RMSD of all the heavy atoms for each of Lys 2, Lys 4, Lys 7, Leu 11, Met 12, Tyr 13, Asp 14, Arg 21, and Lys 24 is greater than 1.1 Å (Figure 5C), indicating that the side chains of these residues are fluctuating in solution. Figure 6D shows the distribution per residue of the order parameter S, indicating the homogeneity of backbone dihedral angles. The majority of the backbone dihedral angles are very well defined ($S > 0.8$), except for those of Gly 3, Met 12, and Tyr 13, which have lower angular order parameters ($S < 0.8$). These residues having a low S value, correspond to N-terminal and loop regions between β-strand 1 and 2 in the calculated tertiary structure.

Description of the Three-Dimensional Structure. Figure 7 shows a stereopair representation of the best-fit superposition of the backbone atoms (N, C^α, C) for 13 converged structures. Analysis of the 13 converged structures indicates that the molecular structure of ω-CTX MVIIA contains a β-sheet region composed of three shortβ-strands, i.e., β-strand 1 (Ala 6 to Cys 8), β-strand 2 (Ser 19 to Arg 21), and β-strand 3 (Lys 24 to Cys 25). It can be classified as a triple-stranded antiparallel β-sheet of topology $+2x$, -1 (Richardson, 1981) as shown in Figure 8. The β-sheet is the best defined region through the entire molecule, as indicated by

Table 1: Structural Statistics for ω-CTX MVIIA[a]

structural parameter	13 converged structures	mean structure
RMS deviations from experimental distance constraints (Å)		
all (251)	0.041 ± 0.004	0.040
intraresidue (89)	0.041 ± 0.006	0.037
sequential (76)	0.046 ± 0.013	0.046
medium range ($\|i - j\| < 5$) (22)	0.053 ± 0.021	0.058
long range ($\|i - j\| \geq 5$) (45)	0.018 ± 0.007	0.019
hydrogen bond and disulfide bond (19)	0.014 ± 0.013	0.028
RMS deviation from experimental dihedral constraints (deg) (22)	0.537 ± 0.222	0.936
energetic statistics (kcal mol^{-1})[b]		
F_{NOE}	21.1 ± 4.4	19.7
F_{tor}	0.43 ± 0.32	0.9
F_{repel}	3.33 ± 1.80	4.5
E_{L-J}	−56.6 ± 6.5	−51.0
RMS deviations from idealized geometry		
bonds (Å)	0.003 ± 0.0004	0.003
angles (deg)	0.319 ± 0.056	0.422
impropers (deg)	0.339 ± 0.053	0.499

[a] The 13 converged structures refer to the final set of dynamic simulated annealing structures starting from 100 initial random structures; the mean structure was obtained by restrained minimization of the averaged coordinate of the 13 individual structures. The number of each experimental constraint used in the calculations is given in parentheses. [b] F_{NOE}, F_{tor}, and F_{repel} are the energies related to the NOE violations, the torsion angle violations, and the van der Waals repulsion term, respectively. The values of the force constants used for these terms are the standard values as depicted in X-PLOR 3.1 manual. E_{L-J} is the Lennard-Jones van der Waals energy calculated with the CHARMm (Brooks et al., 1983) empirical energy functions.

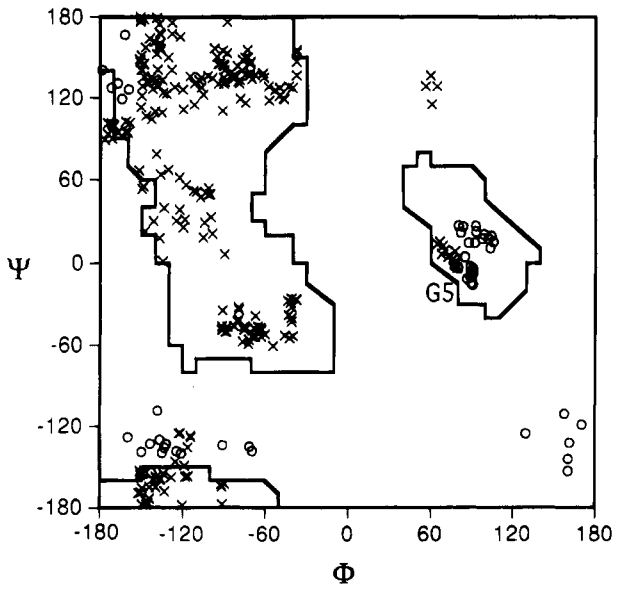

FIGURE 5: Ramachandran plot of the backbone conformational (φ,ψ) angles for all residues of the 13 converged structures of ω-CTX MVIIA. The circles (○) indicate glycine residues and the crosses (×) indicate other residues.

the small values of the corresponding backbone RMSD (Table 2), and the extent of each β-strand is limited by the presence of the characteristic turn structures.

We have identified the turns using the standard definition that the distance between $C^{\alpha}(i)$ and $C^{\alpha}(i+3)$ is less than 7 Å (Lewis et al., 1973) and by evaluating the characteristic distance connectivities of backbone protons (Wüthrich, 1986) for the corresponding turn segments in the 13 final converged structures and their mean structure. These analyses led to the identification of four β-turns which were classified according to Wilmot and Thornton (1990). The four β-turns involve residues Gly 3 to Ala 6 (type II), Ser 9 to Met 12 (type I), Cys 15 to Gly 18 (type VIII), and Hyp 21 to Lys 24 (type I′ hairpin). The average dihedral angles for residues $i+1$ and $i+2$ of these β-turns were $\phi_2 = -90°$, $\psi_2 = 134°$ and $\phi_3 = 106°$, $\psi_3 = -13°$ for Lys 4 and Gly 5, $\phi_2 = -39°$, $\psi_2 = -25°$ and $\phi_3 = -80°$, $\psi_3 = -46°$ for Arg 10 and Leu 11, $\phi_2 = -64°$, $\psi_2 = -48°$ and $\phi_3 = -140°$, $\psi_3 = 151°$ for Cys 16 and Thr 17, and $\phi_2 = 68°$, $\psi_2 = 9°$ and $\phi_3 = 84°$, $\psi_3 = 26°$ for Ser 22 and Gly 23, respectively. These turns are stabilized by the hydrogen bonds between the carbonyl group (i) and the amide proton ($i+3$) of the peptide backbone. The hydrogen−deuterium exchange experiment led to the identification of the slowly exchanging amide protons originating from these four turns. The characteristic φ and ψ angle ranges of β-turns are conserved in all 13 converged structures and show high convergence in a Ramachandran plot.

As described above, the molecular architecture of ω-CTX MVIIA is made up a number of intramolecular hydrogen bonds and three disulfide bonds, resulting in a compact well-defined structure over the entire molecule. The disulfide bonds between Cys 1 and Cys 16 and between Cys 15 and Cys 25 constrain the peptide backbone into a close spatial contact between the third β-turn (Cys 15 to Gly 18) and the N- and C-termini, respectively, and the disulfide bond between Cys 8 and Cys 20 interconnects β-strands 1 and 2. Consequently, the disulfide bonds between Cys 1 and Cys 16 and between Cys 8 and Cys 20 are located at the surface, and the disulfide bond between Cys 15 and Cys 25 is buried in the inside of the molecule.

DISCUSSION

Structural Comparison with the ω-CTX GVIA, Another N-Type Calcium Channel Blocker. In the present study, we have determined the three-dimensional structure of ω-CTX MVIIA in aqueous solution by using ^{1}H NMR spectroscopy and simulated annealing calculations. ω-CTX MVIIA is composed of a short triple-stranded antiparallel β-sheet and several turns. The overall β-sheet topology is $+2x$, -1, which is the same as that reported for ω-CTX GVIA, another N-type calcium channel blocker. As shown in Figure 9A,B, the global conformation of ω-CTX MVIIA is similar to that of the structurally well-characterized ω-CTX GVIA (Davis et al., 1993; Pallaghy et al., 1993; Sevilla et al., 1993;

Table 2: Root Mean Square Differences for the 13 Converged Structures of ω-CTX MVIIA[a]

	atomic RMS differences of 13 converged structures versus mean structure (Å)		average pairwise RMS differences for 13 converged structures (Å)	
	residues 1−25	residues 6−8, 19−21, 24−25	residues 1−25	residues 6−8, 19−21, 24-25
backbone				
(N, C^{α}, C)	0.47 ± 0.08	0.35 ± 0.04	0.68 ± 0.18	0.52 ± 0.12
(N, C^{α}, C, O)	0.54 ± 0.08	0.40 ± 0.05	0.78 ± 0.18	0.58 ± 0.12
all heavy atoms	1.27 ± 0.14	1.22 ± 0.22	1.85 ± 0.28	1.78 ± 0.44

[a] The RMSD values were obtained by best fitting the backbone atoms (N, C^{α}, C, O) coordinates for all the residues of the 13 converged structures. The given numbers for the backbone and all heavy atoms represent the mean values ± standard deviations.

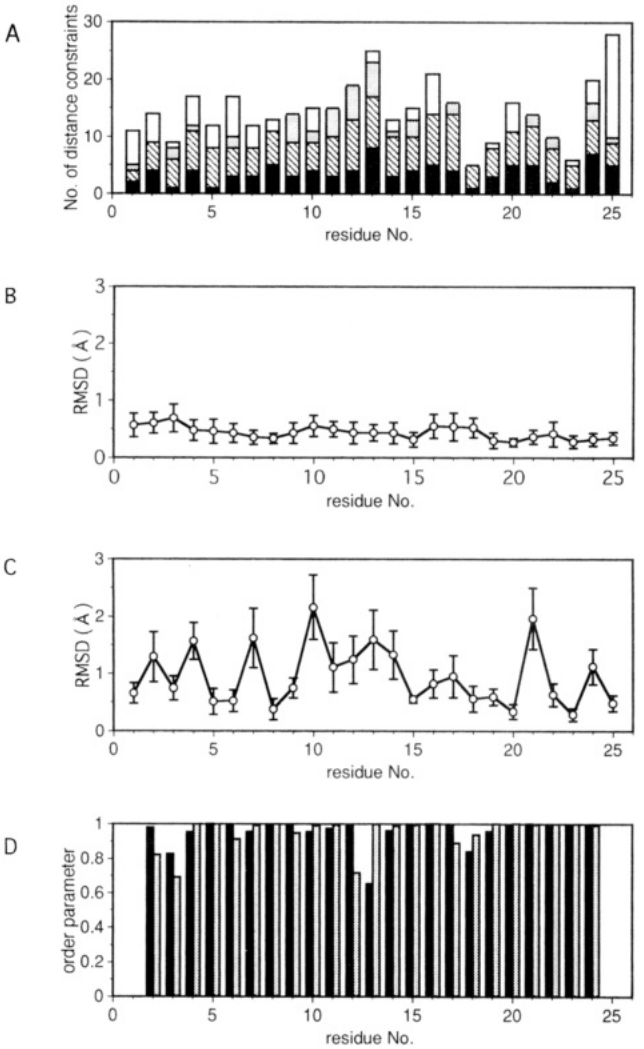

FIGURE 6: Backbone variability by residue. (A) Distribution of the number of experimental distance constraints as a function of the sequence position of ω-CTX MVIIA. Filled bars, intraresidue NOEs; hatched bars, sequential NOEs; stippled bars, medium-range NOEs; open bars, all-long range constraints. (B and C) Distribution of the RMS distance of the backbone (B) and all heavy atoms (C) from the mean structure as a function of residue number is shown together with the standard deviations in these values. (D) Filled bars, the order parameter S of the ϕ; shaded bars, the order parameter S of the ψ, 0 = randomly distributed, and 1 = perfectly aligned.

Skalicky et al., 1993). Despite the relatively low amino acid sequence homology among many ω-conotoxins, the structures of toxins show a similar location and orientation of secondary structure elements in their three-dimensional coordinates. Figure 9C shows the sequential representation of secondary structures found in both molecules with matching of structural positions.

Some differences between the structures come from the length of the β-strands and types of β-turns. The length of the β-strand 1 is the same, but those of the β-strands 2 and 3 in ω-CTX MVIIA are one and two residues shorter, respectively, than those of ω-CTX GVIA. The β-structure in ω-CTX GVIA contains residues Ser 6 to Cys 8 (β-strand 1), Ser 18 to Hyp 21 (β-strand 2), and Lys 24 to Tyr 27 (β-strand 3). The lengths of β-strand 1 and 2 in both structures are limited by the presence of the corresponding β-turns. Interestingly, the Tyr 27 (the last residue of β-strand 3) amide proton of ω-CTX GVIA is hydrogen-bonded to the carbonyl group of Ser 18 (in β-strand 2), whereas the corresponding hydrogen bond of ω-CTX MVIIA is formed between the C-terminal NH_2 and Ser 19 (in β-strand 2). In both cases, however, these hydrogen bonds were not identified in hydrogen−deuterium exchange experiments, as proton donors located at the C-terminus have close contact with solvent. In the case of ω-CTX MVIIA, the presence of this hydrogen bond is supported by the average distance of 2.1 Å and by the NOE cross peak between C-terminal NH_2 and $C_{\alpha}H$ of Cys 20 (element of β-strand 2).

The β-turns are essential for the formation of the globular structure of ω-CTX MVIIA and ω-CTX GVIA . In the case of ω-CTX GVIA, it is composed of the four β-turns involving residues Ser 3 to Ser 6 (type II), Ser 9 to Ser 12 (type I), Cys 15 to Ser 18 (type I or VIII), and Hyp 21 to Lys 24 (hairpin). As shown in Figure 9C, the first, second and third turns of the two molecules, as numbered from the N-terminus, have almost the same β-turn conformations, i.e., type II, type I, and type VIII, respectively. As indicated by Davis et al. (1993), the first turn of the toxin molecules takes on a type II β-turn, in which the glycine residue at position 5 is conserved in all known ω-conotoxins, suggesting that the same type of turn is also conserved among ω-conotoxins. However, there is a significant difference between the structures with respect to the fourth turns connecting the β-strands 2 and 3. In the case of ω-CTX GVIA, the fourth turn is formed by a hairpin turn between Hyp 21 and Lys 24 (Davis et al., 1993), in which the averaged dihedral angles for residues Tyr 22 and Thr 23 are $\phi_2 = -62°$, $\psi_2 = -44°$ and $\phi_3 = -103°$, $\psi_3 = -6°$, respectively; therefore, it constitutes a the type I β-turn. In contrast, the ω-CTX MVIIA hairpin turn (Arg 21 to Lys 24) belongs to the type I′ β-turn. For β-hairpins, type I′ turns are more common than type I turns. In hairpins, type I′ turns have the correct twist to match the relative twist between adjacent strands, whereas its mirror image (type I) has an energetically less favorable incorrect twist (Sibanda & Thronton, 1985). The glycine at position 23 (ω-CTX MVIIA) is a dominant residue of the type I′ hairpin turn. The type I hairpin turn found in ω-CTX GVIA may be attributed to the formation of unusual

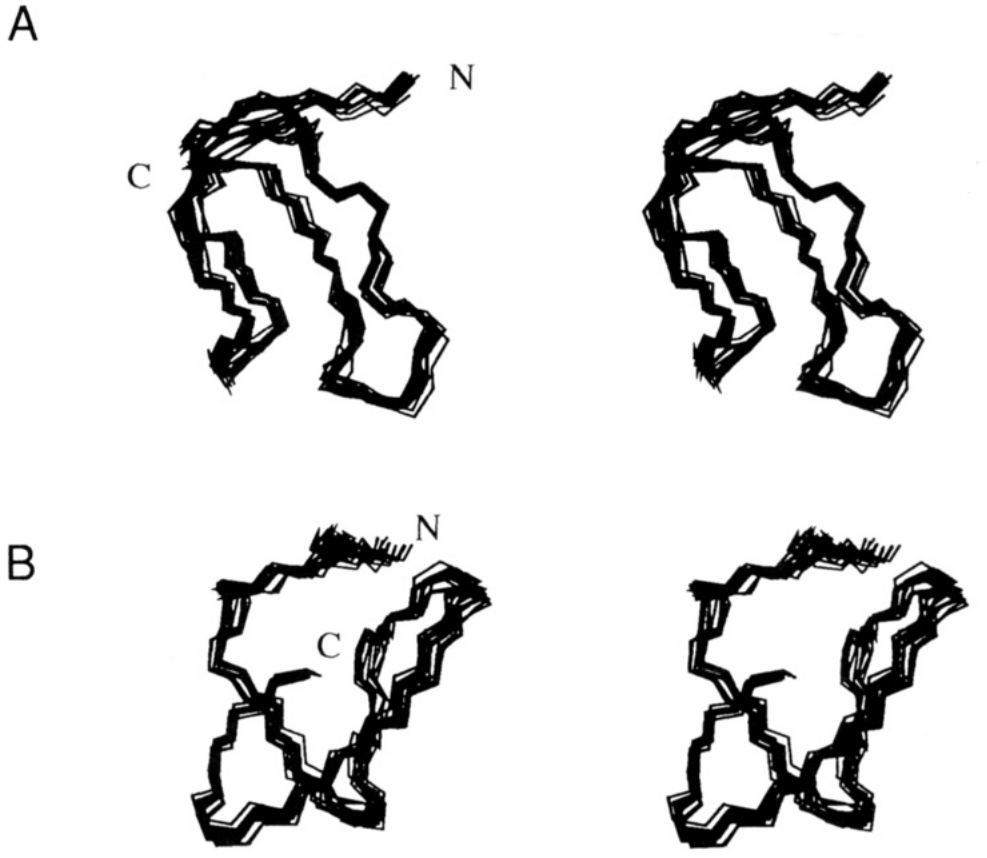

FIGURE 7: Stereopairs of backbone heavy atoms (N, C^{α}, and C) for the 13 converged structures of ω-CTX MVIIA. These are the results of the best-fit superposition of the backbone atoms (N, C^{α}, C, and O) for all the residues of the molecule. (A) Stereopair for the complete sequence. (B) Stereopair for the complete sequence obtained by a 90° rotation about the vertical axis of stereopair A.

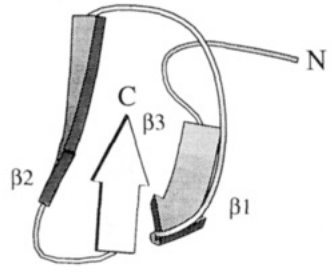

FIGURE 8: MOLSCRIPT (Kraulis, 1991) diagram of the backbone polypeptide folding of ω-CTX MVIIA. The structural topology of the triple-stranded antiparallel β-sheet is shown.

hydrogen bonds by the carbonyl side chain group of Asn 20 (Davis et al., 1993).

Consequently, certain differences in the secondary structure of the two toxins might reflect differences in the total number of amino acids between the fourth Cys and the amidated C-terminus. The number of residues between the fourth and fifth Cys and between the fifth and sixth Cys is three and four residues for ω-CTX MVIIA and two and six residues for ω-CTX GVIA, respectively. Thus, ω-CTX MVIIA has one insertion and two deletions in the intercysteine regions between the fourth and fifth Cys and between the fifth and sixth Cys, respectively.

Conus venoms contain a family of toxins of 24−29 amino acids in length, related to ω-conotoxin, and all of them have the same conserved cysteine framework in the primary sequence (Olivera et al., 1994). The three disulfide bonds play a crucial role in maintaining the biologically active conformation of ω-conotoxins. In the case of ω-CTX GVIA, changes in the number and the pairings of disulfide bonds resulted in partial disruption of the biologically active structure, leading to a reduction of the channel-blocking activity (Pennington et al., 1992; Sabo et al., 1992). Pallaghy et al. (1993) indicated that the structure of disulfide isomers displays some conformational heterogeneity in solution with significant loss of the structural features of the native molecule. Furthermore, linear analogs of ω-CTX MVIIA and ω-CTX GVIA, with full deletion of three disulfide bonds, showed a complete loss in their binding affinity for N-type calcium channels.

The results described above suggest that the structurally conserved disulfide bonds as well as the overall molecular folding, including the location of three β-strands and four β-turns in the three-dimensional structures of both molecules, significantly contribute to maintaining a biologically active conformation.

Structure−Function Relationships of ω-Conotoxins. Many kinds of ω-conotoxins have been reported. They have been classified into several groups on the basis of their specificity for calcium channel subtypes. Among the conotoxins from *C. magus*, ω-CTX MVIIA binds to N-type calcium channels whereas ω-CTX MVIIC binds to Q-type calcium channels, although sequence homology between these two toxins is rather high (Figure 1). On the other hand, ω-CTX GVIA from *C. geographus* has low sequence homology with ω-CTX MVIIA even though both bind to N-type calcium channels. We have determined that the side chain of Tyr 13 is crucial for the calcium channel binding activity of both ω-CTX MVIIA and ω-CTX GVIA (Kim et al., 1994, 1995). Probably only a few amino acid side chains are important for interaction with N-type calcium channels and the location

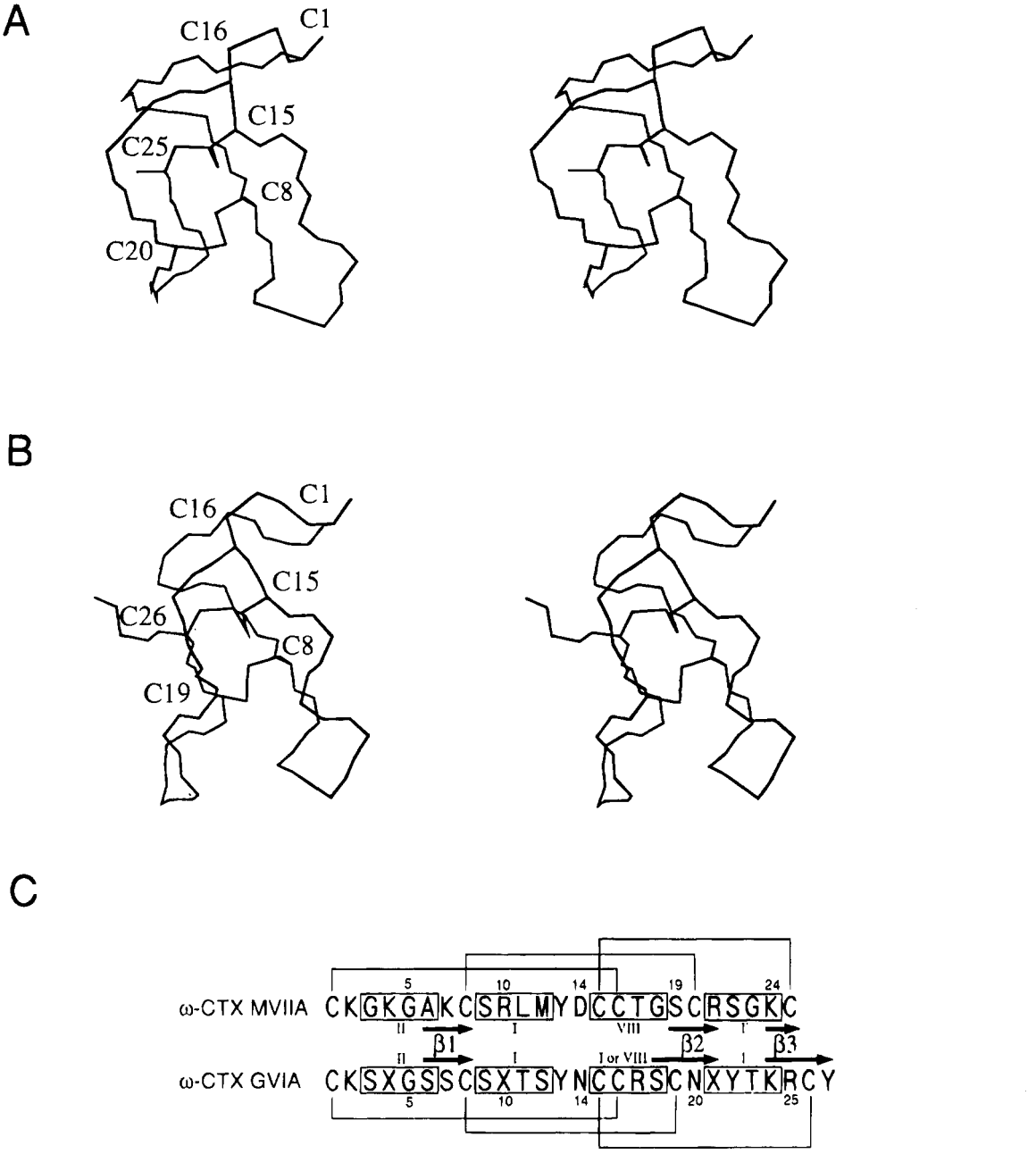

FIGURE 9: Stereopairs of NMR solution structure of two calcium channel blockers. (A) Mean structure of ω-CTX MVIIA having three disulfide bonds of Cys 1− Cys 16, Cys 8−Cys 20, and Cys 15−Cys 25. (B) Refined structure of ω-CTX GVIA having three disulfide bonds of Cys 1−Cys 16, Cys 8−Cys 19, and Cys 15−Cys 26. (C) Comparative arrangements of amino acid sequences based on the distribution of secondary structure elements and three disulfide bonds of ω-CTX MVIIA and ω-CTX GVIA. Hydroxyproline residues in ω-CTX GVIA are denoted as X in single-letter amino acid abbreviations. Arrows and squares represent the β-strands and β-turns in the solution structures of the two peptide toxins, respectively. The disulfide connectivities are indicated by the horizontal lines. The ω-CTX GVIA structure coordinates were extracted from the Brookhaven Protein Data Bank entry 1OMC.

of the single most important residue, Tyr 13, is conserved between both toxins as shown in Figure 10. As for the conformation around Tyr 13, a comparison of the order parameter S with the RMSD data (see Figure 6B−D) allows an interesting observation. From the data of the single-residue backbone RMSD (Figure 6B), the entire backbone structure including Tyr 13 is well defined. However, order parameter S indicates that Tyr 13 is included in the region where the parameter is the lowest in the structure (Figure 6D). This is also the case with the calculated structure of ω-CTX GVIA (Davis et al., 1993). These data may show that the backbone region around Tyr 13 is rather flexible around the ϕ and ψ angles. Perhaps, this flexibility around ϕ and ψ may help to rotate and locate the side chain of Tyr 13 into the appropriate position to confer activity.

In the case of ω-CTX GVIA, Lys 2 is a second important residue for calcium channel binding as we reported previously (Sato et al., 1993). Although this lysine residue is conserved in ω-CTX MVIIA, it only has a minor role in calcium channel binding (Kim et al., 1995). Probably as ω-CTX MVIIA has a greater net charge (+6) than that of ω-CTX GVIA (+5), the role of Lys 2 may be fulfilled by some other basic residue. The calculated structure in this study suggests that Lys 7 may be a candidate. Figure 10C shows the location of Lys 2, Lys 4, and Lys 7 in the average structure of ω-CTX MVIIA. The side chain of Lys 7 extends

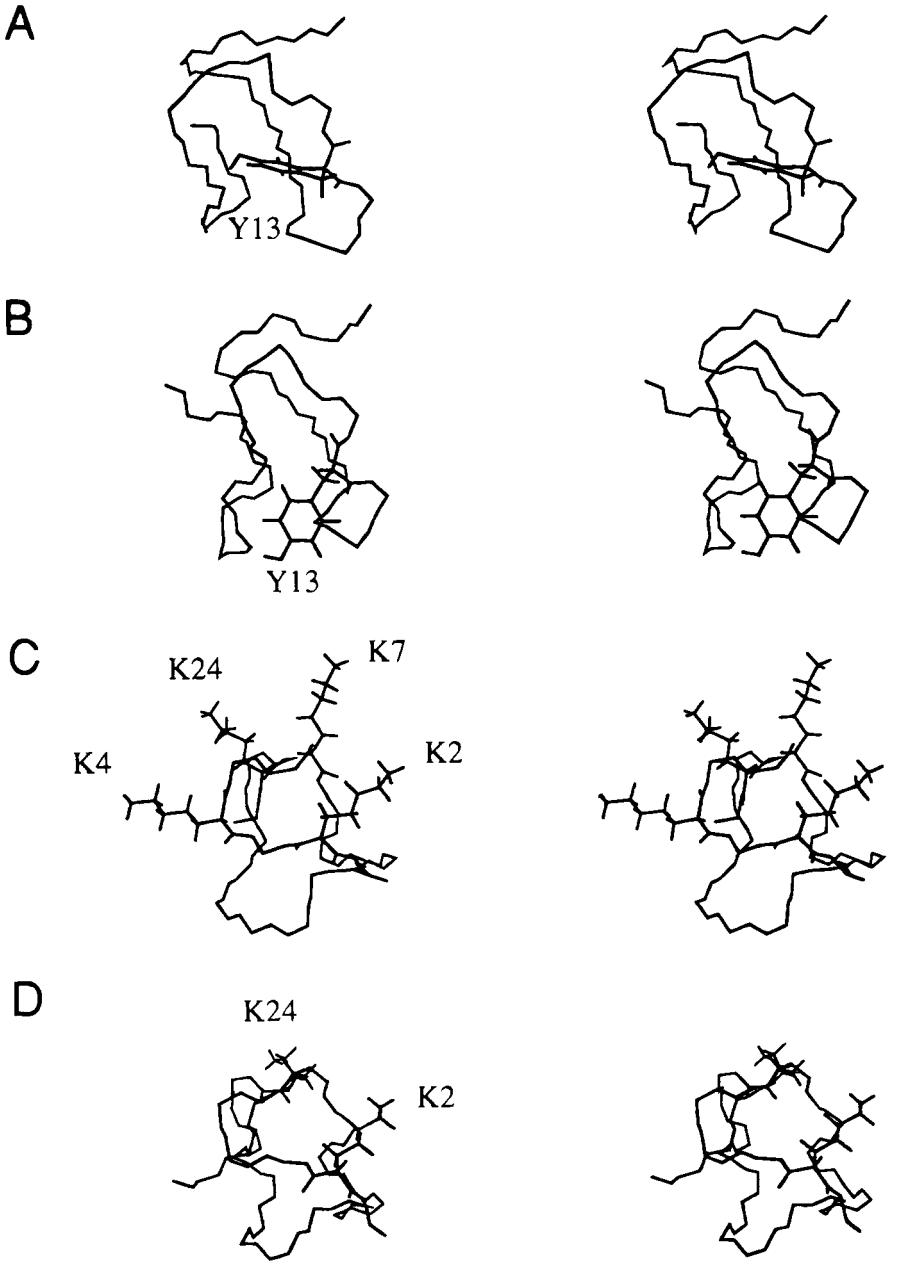

FIGURE 10: (A) Mean structure of ω-CTX MVIIA representing Tyr 13, the most important residue for calcium channel binding activity. (B) Mean structure of ω-CTX GVIA representing Tyr 13. (C) Mean structure of ω-CTX MVIIA representing all four lysine residues, Lys 2, Lys 4, Lys 7, and Lys 24. (D) Mean structure of ω-CTX GVIA representing the two lysine residues, Lys 2 and Lys 24. Panels A and B correspond to the orientation of the molecule shown in Figure 9, panels A and B, respectively. Panels C and D are obtained by a 90° rotation about the horizontal axis of the stereopairs in Figure 9, panels A and B, respectively.

in the same direction as that of Lys 2, whereas Lys 4 is orientated in the opposite direction. The seventh residue in the primary structure of ω-CTX GVIA is Ser 7, which is not a basic amino acid. This suggests that Lys 2 and/or Lys 7 may play an important role in the activity and Lys 7 may compensate Lys 2 when Lys 2 is replaced with an alanine residue. To determine the role of these lysine residues in more detail, the activity of an ω-CTX MVIIA analog in which both Lys 2 and Lys 7 are replaced with other amino acid residues should be measured.

A characteristic of ω-CTX GVIA is the presence of three hydroxyproline (Hyp) residues. Hyp 4 and Hyp 10 are in the second position of a β-turn, and Hyp 21 is in the junction between the second β-strand and the hairpin turn. Hydroxyl groups of Hyp residues in ω-CTX GVIA are not necessary for calcium channel binding, since activity was retained when all three Hyp residues were simultaneously replaced with Pro residues (Kim et al., 1994). Due to their cyclic structure, Hyp residues are expected to be important for disulfide bond formation in the folding reaction (Sato et al., 1991). In the case of ω-CTX GVIA, however, three analogs in which an Ala residue was substituted for each Hyp residue folded smoothly in chemical synthesis (J. I. Kim et al., unpublished results), suggesting that none of the three Hyp residues is essential for the folding of the molecule. Although ω-CTX MVIIA has no Hyp or Pro residue, it takes on a three-dimensional structure similar to that of ω-CTX GVIA, suggesting that Hyp residues are not required to determine the three-dimensional structure of ω-conotoxins. Hydroxyl groups of Hyp residues in ω-CTX GVIA may improve the solubility of this molecule, since [Pro^{4,10,21}]ω-CTX GVIA was less soluble than ω-CTX GVIA. In the case of ω-CTX

MVIIA, the amino acids corresponding to Hyp residues in ω-CTX GVIA are Lys 4, Arg 10, and Arg 21. All of them are basic hydrophilic amino acid residues. This is also the case with ω-CTX MVIIC which has Lys residues at the fourth and tenth positions.

ω-CTX MVIIC shares nearly 70% sequence homology with ω-CTX MVIIA; however, their pharmacological specificity is very different. The overall conformations of these toxins are similar to each other, so their difference in specificity may depend on the residues which are not conserved. Among the conserved residues, position 13 may be essential for binding to both N- and Q-type calcium channels. The determinants for binding to Q-type calcium channels may be among the residues which are neither conserved between ω-CTX MVIIC and MVIIA nor between ω-CTX MVIIC and GVIA. From this point of view, the candidates are Pro 7, Arg 9, Lys 10, Ser 17, Gly 21, Arg 22, and Arg 23 in ω-CTX MVIIC. It is interesting that many of the candidates are basic residues. To discuss in more detail, the analogs in which candidate residues are replaced with other residues should be examined.

The solution structure of ω-conotoxin reported here should contribute to our understanding of the structure and action of calcium channel blockers and be useful in designing synthetic organic compounds with selective antagonist or agonist action at differenct calcium channel subtypes.

ACKNOWLEDGMENT

We thank Dr. Masami Takahashi for discussion and Dr. Michael J. Seagar for critical reading of the manuscript.

SUPPORTING INFORMATION AVAILABLE

One table of ^{1}H NMR chemical shifts of ω-CTX MVIIA (2 pages). Ordering information is given on any current masthead page.

REFERENCES

Adams, M. E., & Olivera, B. M. (1994) *Trends Neurosci. 17*, 151−155.
Bax, A., & Davis, D. G. (1985) *J. Magn. Reson. 65*, 355−359.
Birnbaumer, L., Campbell, K. P., Catterall, W. A., Harpold, M. M., Hofman, F., Horne, W. A., Mori, Y., Schwartz, A., Snutch, T. P., Tanabe, T., & Tsien, R. W. (1994) *Neuron 13*, 505−506.
Brooks, B. R., Bruccoleri, R. E., Olafson, B. D., States, D. J., Swaminathan, S., & Karplus, M. (1983) *J. Comput. Chem. 4*, 187−217.
Brünger, A. T. (1993) *X-PLOR Manual,* Version 3.1, Yale University, New Haven, CT.
Clore, G. M., Gronenborn, A. M., Nilges, M., & Ryan, C. A. (1987) *Biochemistry 26*, 8012−8023.
Davis, J. H., Bradley, E. K., Miljanich, G. P., Nadasdi, L., Ramachandran, J., & Basus, V. J. (1993) *Biochemistry 32*, 7396−7405.
Hyberts, S. G., Marki, W., & Wagner, G. (1987) *Eur. J. Biochem. 164*, 625−635.
Hyberts, S. G., Goldberg, M. S., Havel, T. F., & Wagner, G. (1992) *Protein Sci. 1*, 736−751.
Jeener, J., Meier, B. H., Bachmann, P., & Ernst, R. R. (1979) *J. Chem. Phys. 71*, 4546−4553.
Kim, J.-I., Takahashi, M., Ogura, A., Kohno, T., Kudo, Y., & Sato, K. (1994) *J. Biol. Chem. 269*, 23876−23878.
Kim, J.-I., Takahashi, M., Ohtake, A., Wakamiya, A., & Sato, K. (1995) *Biochem. Biophys. Res. Commun. 206*, 449−454.
Kraulis, P. (1991) *J. Appl. Crystallogr. 24*, 946−950.
Lewis, P. N., Momany, F. A., & Scherega, H. A. (1973) *Biochim. Biophys. Acta 303*, 211−229.
Macura, S., Huang, Y., Suter, D., & Ernst, R. R. (1981) *J. Magn. Reson. 43*, 259−281.
Marion, D., & Wüthrich, K. (1983) *Biochem. Biophys. Res. Commun. 113*, 967−974.
Mueller, L. (1987) *J. Magn. Reson. 72*, 191−196.
Nilges, M., Clore, G. M., & Gronenborn, A. M. (1988) *FEBS Lett. 229*, 317−324.
Olivera, B. M., McIntosh, J. M., Cruz, L. J., Luque, F. A., & Gray, W. R. (1984) *Biochemistry 23*, 5087−5090.
Olivera, B. M., Cruz, L. J., Santos, V. d., LeCheminant, G. W., Griffin, D., Zeikus, R., McIntosh, J. M., Galyean, R., Varga, J., Gray, W. R., & Rivier, J. (1987) *Biochemistry 26*, 2086−2090.
Olivera, B. M., Miljanich, G. P., Ramachandran, J., & Adams, M. E. (1994) *Annu. Rev. Biochem. 63*, 823−867.
Pallaghy, P. K., Duggan, B. M., Pennington, M. W., & Norton, R. S. (1993) *J. Mol. Biol. 234*, 405−420.
Pardi, A., Billerter, M., & Wüthrich, K. (1984) *J. Mol. Biol. 180*, 741−751.
Pennington, M. W., Fetsin, S. M., Maccecchini, M. L., & Kem, W. R. (1992) *Toxicon 30*, 755−764.
Ramachandran, G. N., Ramakrishnan, C., & Sasisekharan, V. (1963) *J. Mol. Biol. 7*, 95−99.
Rance, M., Sørensen, O. W., Bodenhausen, G., Wagner, G., Ernst, R. R., & Wüthrich, K. (1983) *Biochem. Biophys. Res. Commun. 117*, 479.
Richardson, J. S. (1981) *Adv. Protein Chem. 34*, 167−339.
Sabo, T., Gilon, C., Shafferman, A., & Elhanaty, E. (1992) in *Peptides: Chemistry and Biology. Proceedings of the 12th American Peptide Symposium*, pp 159−160, Escom Science Publshers, Leiden, The Netherlands.
Sato, K., Ishida, Y., Wakamatsu, K., Kato, R., Honda, H., Ohizumi, Y., Nakamura, H., Ohya, M., Lancelin, J.-M., Kohda, D., & Inagaki, F. (1991) *J. Biol. Chem. 266*, 16989−16991.
Sato, K., Park, N.-G., Kohno, T., Maeda, T., Kim, J.-I., Kato, R., & Takahashi, M. (1993) *Biochem. Biophys. Res. Commun. 194*, 1292−1296.
Sevilla, P., Bruix, M., Santoro, J., Gago, F., Carcia, A. G., & Rico, M. (1993) *Biochem. Biophys. Res. Commun. 192*, 1238−1244.
Sibanda, B. L., & Thronton, J. M. (1985) *Nature 316*, 170−174.
Skalicky, J. J., Metzler, W. J., Ciesla, D. J., Galdes, A., & Pardi, A. (1993) *Protein Sci. 2*, 1591−1603.
Wagner, G., Braun, W., Havel, T. F., Schaumann, T., Go, N., & Wüthrich, K. (1987) *J. Mol. Biol. 196*, 611−639.
Wilmot, C. M., & Thornton, J. M. (1990) *Protein Eng. 3*, 479−493.
Wishart, D. S., Sykes, B. D., & Richards, F. M. (1992) *Biochemistry 31*, 1647−1651.
Wüthrich, K. (1986) *NMR of Proteins and Nucleic Acids*, Wiley, New York.
Wüthrich, K., Billeter, M., & Braun, W. (1983) *J. Mol. Biol. 169*, 949−961.
Wüthrich, K., Billeter, M., & Braun, W. (1984) *J. Mol. Biol. 180*, 715−740.

BI950757G